




Cardiac sympathetic innervation network shapes the myocardium by locally controlling cardiomyocyte size through the cellular proteolytic machinery

Nicola Pianca^{1,2}, Anna Di Bona^{1,3,*}, Erica Lazzeri^{4,*}, Irene Costantini^{4,5}, Mauro Franzoso^{1,2}, Valentina Prando^{1,3} , Andrea Armani^{1,2}, Stefania Rizzo³, Marny Fedrigo³, Annalisa Angelini³, Cristina Basso³, Francesco S. Pavone^{4,5,6}, Michael Rubart⁷, Leonardo Sacconi^{4,5} , Tania Zaglia^{1,2,3,†} and Marco Mongillo^{1,2,8,†} 

¹Veneto Institute of Molecular Medicine, Padova, Italy

²Department of Biomedical Sciences, University of Padova, Padova, Italy

³Department of Cardiac, Thoracic, Vascular Sciences and Public Health, University of Padova, Padova, Italy

⁴European Laboratory for Non-linear Spectroscopy, University of Florence, Florence, Italy

⁵National Institute of Optics, National Research Council, University of Florence, Florence, Italy

⁶Department of Physics and Astronomy, University of Florence, Florence, Italy

⁷Indiana University School of Medicine, Indianapolis, IN, USA

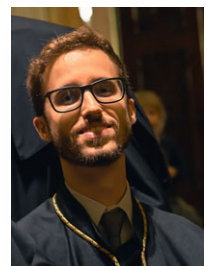
⁸CNR Institute of Neuroscience, Padova, Italy

Edited by: Don Bers & Bjorn Knollmann

Key points

- The heart is innervated by a dense sympathetic neuron network which, in the short term, controls chronotropy and inotropy and, in the long term, regulates cardiomyocyte size. Acute neurogenic control of heart rate is achieved locally through direct neuro-cardiac coupling at specific junctional sites (neuro-cardiac junctions).
- The ventricular sympathetic network topology is well-defined and characteristic for each mammalian species.
- In the present study, we used cell size regulation to determine whether long-term modulation of cardiac structure is achieved via direct sympatho-cardiac coupling.
- Local density of cardiac innervation correlated with cell size throughout the myocardial walls in all mammalian species analysed, including humans.
- The data obtained suggest that constitutive neurogenic control of cardiomyocyte trophism occurs through direct intercellular signalling at neuro-cardiac junctions.

Nicola Pianca received his PhD in Bioscience and Biotechnology from the University of Padova. His studies focus on neuro-cardiology and cardiomyocyte proteostasis. He specializes in a broad range of experimental techniques, including cardiac optogenetics, which he has used to study the tissue determinants of arrhythmias in the diseased heart.



*These authors contributed equally to this work.

†These authors contributed equally to this work.

Abstract It is widely appreciated that sympathetic stimulation of the heart involves a sharp increase in beating rate and significant enhancement of contractility. We have previously shown that, in addition to these evident functions, sympathetic neurons (SNs) also provide trophic input to cardiomyocytes (CMs), regulating cell and organ size. More recently, we have demonstrated that cardiac neurons establish direct interactions with CMs, allowing neuro-cardiac communication to occur locally, with a 'quasi-synaptic' mechanism. Based on the evidence that cardiac SNs are unevenly distributed throughout the myocardial walls, we investigated the hypothesis that CM size distribution reflects the topology of neuronal density. *In vitro* analyses of SN/CM co-cultures, *ex vivo* confocal and multiphoton imaging in clarified hearts, and biochemical and molecular approaches were employed, in both rodent and human heart biopsies. In line with the trophic effect of SNs, and with local neuro-cardiac communication, CMs, directly contacted by SNs in co-cultures, were larger than the non-targeted ones. This property reflects the distribution of CM size throughout the ventricles of intact mouse heart, in which cells in the outer myocardial layers, which were contacted by more neuronal processes, were larger than those in the less innervated subendocardial region. Such differences disappeared upon genetic or pharmacological interference with the trophic SN/CM signalling axis. Remarkably, CM size followed the SN distribution pattern in other mammals, including humans. Our data suggest that both the acute and chronic influence of SNs on cardiac function and structure is enacted as a result of the establishment of specific intercellular neuro-cardiac junctions.

(Received 31 January 2019; accepted after revision 21 May 2019; first published online 22 May 2019)

Corresponding author T. Zaglia: Department of Cardiac, Thoracic, Vascular and Public Health, University of Padova, via Giustiniani 2, 35128 Padova, Italy. E-mail: tania.zaglia@unipd.it

M. Mongillo: Department of Biomedical Sciences, University of Padova, Via Ugo Bassi 58/B, 35122 Padova, Italy & Veneto Institute of Molecular Medicine, via Orus, 2 35129 Padova, Italy. E-mail: marco.mongillo@unipd.it

Introduction

The myocardium comprises a complex network of different cell types, which finely co-operate to ensure repeated and adjustable blood ejection and match the perfusional demands during any given physiological state (Bers & Despa, 2009; Liu *et al.*, 1993). In addition to the intrinsic adaptation to mechanical load (i.e. pre- and after-load), the sympathetic nervous system has been classified as the most important extrinsic regulator of cardiac function (Levy, 1997; Iriki & Simon, 2012). Such a view stems from more than 200 years of studies that have addressed the gross anatomy of nerves directed to the heart, as well as the effect (as is self-evident throughout species) of acute sympathetic neuron (SN) activation on the abrupt increase of contraction and rate (Gros *et al.*, 1994; Guyton & Hall, 2006; Zipes, 2008; May *et al.*, 2010). The fine anatomy and interactions between neurons and myocardial targets have only started to be appreciated much later, in parallel with the development and widespread use of β -adrenoceptor (β -AR) blockers (Nattel *et al.*, 1979; Clarke *et al.*, 2010). This has uncovered the emerging functions of SNs, spanning from the tuning of heart rate variability (Eckberg, 2000; Li *et al.*, 2000; Thayer *et al.*, 2012) and the regulation of cell cycle to the modulation of cardiomyocyte (CM) proteostasis (Ogawa *et al.*, 1992; Zaglia *et al.*, 2013; Kreipke & Birren, 2015). By analysing the heart upon chemical ablation

of cardiac innervation, we have shown that SNs provide trophic input to CMs, as enacted through the downstream effects of noradrenaline (NE)-activated β_2 -ARs on the expression of muscle specific ubiquitin ligases, including MuRF-1. Indeed, denervated hearts activate the atrophic programme, which was operated in the early phases by the ubiquitin/proteasome system and then subsequently followed by activation of the autophagy/lysosome system, accompanied by the probable decrease in protein synthesis (Zaglia *et al.*, 2013).

More recently, we have investigated the biophysics of neuro-cardiac signalling, aiming to address whether the neuronal effects on the heart were the result, in accordance with the archetypal description of cardiac physiology, of the unabridged propagation of sympathetic neurotransmitters throughout the myocardium, or whether neuro-cardiac communication was confined to specific junctional sites, similar to those involved in skeletal muscle contraction (Hall & Sanes, 1993; Homan & Meriney, 2018). This latter hypothesis arose from the results of several previous studies obtained *in vitro* (Chun & Patterson, 1977; Shcherbakova *et al.*, 2007; Oh *et al.*, 2016) and *ex vivo* (Fukuda *et al.*, 2015), suggesting that specific sympathetic synapses may exist in the heart. By applying SN optogenetics, we demonstrated *in vivo* that neurotransmission underlying the rapid and efficient chronotropic effect of SN activation depended on the local release of NE at the intercellular contact site, with features

typical of synaptic transmission (Prando *et al.*, 2018). Such a proof-of-principle demonstration focused on the acute sympathetic regulation of heart rate and the work *in vivo* was therefore limited to the analysis of sino-atrial node (SAN) function. However, close neuro-cardiac appositions were observed in the ventricles and, together with our previous research, this raised the question of whether signalling through neuro-cardiac junctions (NCJs) was also responsible for long-term modulation of cell size in ventricular CMs.

Additionally, cardiac neurons are densely and unevenly distributed throughout the myocardial walls, with a non-random pattern, which has been well characterized in the heart of mice (Freeman *et al.*, 2014; Fukuda *et al.*, 2015), although this still remains largely underappreciated in humans.

Altogether, this prompted us to follow-up our recent work (Prando *et al.*, 2018) and assess whether CM size distribution in the ventricles reflects the topology of cardiac sympathetic innervation.

To assess this hypothesis, we combined *in vitro* analyses of SN/CM co-cultures, with *ex vivo* histological [immunofluorescence (IF)], confocal and multiphoton imaging of clarified hearts, as well as physiological [denervation with 6-hydroxydopamine (6-OH-DA)], biochemical [western blotting (WB), co-immunoprecipitation] and molecular biological [quantitative RT-PCR, *in situ* hybridization (ISH)] approaches, in both rodent and human heart biopsies.

Methods

All of the investigators involved in the present study understand the ethical principles under which the journal operates and the work conducted complies with the animal ethics checklist of *The Journal of Physiology* (Grundy, 2015).

Human samples

Here, we analysed sections from one 2-month-old and one adult subject who had both died as a result of non-cardiac causes. Heart samples were acquired during routine post-mortem clinical investigations and archived in the historical collection of the Institute of Pathological Anatomy of the University of Padova. Samples were anonymous to the investigators and used in accordance with the directives of the national committee of Bioethics and *Raccomandazione (2006) della Commissione dei Ministri degli Stati Membri sull'utilizzo di campioni biologici di origine umana per scopi di ricerca [Recommendation of the Committee of the Ministers of EU member states on the use of samples of human origin for research]*.

Ethical approval

Experimental procedures have been approved by Ministry of Health (Ufficio VI), in compliance with the Animal Welfare Legislation (protocols A06E0.N.ERD and A06E0.18).

All procedures were performed by trained personnel with documented formal training and previous experience in experimental animal handling and care. All of the procedures were refined prior to starting the study, and the number of animals was calculated to use the least number of animals sufficient according to statistical sample power calculations.

Origin and source of animals

In the present study, we analysed hearts from: post-natal day (P)1, P7 and P21 CD1 and C56BL/6J mice, as well as adult (3 months old) CD1 and C57BL/6J male mice (all from Charles River, Milan, Italy). In addition, we used MuRF1 knockout (KO) (Dr David J. Glass, Novartis Institute for Biomedical Research, Cambridge, MA, USA) and α -MyHC-ChR2 (Zaglia *et al.*, 2015) adult (3 months old) male mice. Hearts from Sprague–Dawley adult (2 months old) male rat and rabbit hearts (all from Harlan, Milan, Italy) were also evaluated. Animals were maintained in individually ventilated cages in an Authorized Animal Facility (authorization number 175/2002A) under a 12:12 h light/dark photocycle at a controlled temperature and had access to water and food available *ad libitum*.

SN/CM co-cultures

SN/CM co-cultures were prepared and maintained for 15 consecutive days, as described previously Prando *et al.* (2018). Co-cultures were treated, for 5 consecutive days before fixation, with 1 μ M nicotine (Sigma-Aldrich, St Louis, MO, USA).

SN-cardiac fibroblast (CF) co-cultures

CFs were obtained from neonatal rat hearts, in accordance with the same protocol used for CMs, by short-time plating of the digested tissue on plastic plates. Mixed co-cultures were established by plating CM in the central area of the SN-containing coverslip, and CF in the surrounding area. Cells were cultured in the CM culture medium, supplemented with 10 ng mL⁻¹ nerve growth factor (Sigma-Aldrich).

Live cell imaging of neuro-cardiac co-cultures

Cells seeded on glass coverslips and maintained in the culture plate were imaged every 30 min for up to 6 h using

a custom modified microscope (Nikon, Tokyo, Japan) equipped with a 5D MII digital camera (Canon, Tokyo, Japan).

Mouse pharmacological sympathectomy

Pharmacological sympathectomy was achieved with 6-OH-DA (Sigma-Aldrich) injection. The drug was delivered to adult (3 months old) mice (100 mg kg^{-1} , I.P.), at days 0, 2 and 7. Animals were killed 1, 8 or 30 days after the first 6-OH-DA injection. For permanent heart denervation, the drug was delivered at postnatal days 2, 4, 6, 8 and 9 (70 mg kg^{-1} , I.P.). Denervated animals were sacrificed, by cervical dislocation, at postnatal days 1, 7, 21 and 90. In both experimental groups, control mice were treated with vehicle (0.9% NaCl solution supplemented with 0.1% ascorbic acid) (Zaglia *et al.*, 2013).

In vivo delivery of β 2-AR modulating drugs

The β 2-AR antagonist, ICI 118,551 ($1 \text{ mg kg}^{-1} \text{ day}^{-1}$) or the β 2-AR agonist, clenbuterol ($3 \text{ mg kg}^{-1} \text{ day}^{-1}$) (all from Sigma) were delivered to normal adult (3 months old) male mice by s.c. osmotic mini-pumps (model 1004; Alzet, Cupertino, CA, USA), as described previously (Zaglia *et al.*, 2013), delivering drugs at a constant rate for 14 consecutive days. For mini-pump implantation, mice were anaesthetized with isoflurane (2.5% in O_2), secured to the operating table in prone position, a 1 cm incision was made in the interscapular region, s.c. muscles were dissected and the osmotic mini-pumps inserted s.c. Body temperature and respiratory rate were constantly monitored during the procedure. The mice were left to awaken from anaesthesia under a heating lamp, and were administered a single injection of tramadol (7 mg kg^{-1} , I.M.) in the perioperative phase. At the end of the experiment, mice were killed by cervical dislocation, and their hearts were harvested and processed for IF and morphometric analyses.

Caloric restriction

Adult (3 months old) male mice underwent caloric restriction for 7 days, as described previously (Zaglia *et al.*, 2013). At day 8, mice were killed by cervical dislocation, and their hearts were harvested and processed for IF and morphometric analyses.

IF analysis of the human myocardium

Formalin-fixed paraffin-embedded human heart sections ($3 \mu\text{m}$ thick) underwent antigen retrieval and IF staining, as described previously (Zaglia *et al.*, 2016).

Immunofluorescence analysis of rodent hearts and cells

Hearts were harvested, fixed in 1% paraformaldehyde (PFA) (w/v in $1 \times \text{PBS}$; Sigma Aldrich) and processed, as described previously (Zaglia *et al.*, 2013). Cryosections ($10 \mu\text{m}$ thick) were obtained using a cryostat (model 1860; Leica Microsystems, Wetzlar, Germany) and processed for IF, as described previously (Zaglia *et al.*, 2013). For *in vitro* experiments, cells were fixed with 3.7% formaldehyde (Sigma-Aldrich) at 4°C for 30 min, permeabilized with 0.1% Triton (v/v in $1 \times \text{PBS}$; Sigma-Aldrich) for 5 min and incubated with the primary antibody for 2 h at 37°C . The primary antibodies used in the study were: anti- α -actinin (dilution 1:200; Sigma-Aldrich); anti-tyrosine hydroxylase (anti-TOH; dilution 1:400; Millipore, Billerica, MA, USA); and anti-dystrophin (dilution 1:500; Abcam, Cambridge, MA, USA). Primary antibodies were revealed with 488- or Cy3-conjugated secondary antibodies (all from Jackson Laboratories, Bar Harbor, ME, USA). In a subset of experiments, sections were stained with fluorescein isothiocyanate (FITC)-conjugated wheat germ agglutinin.

Two photon imaging of whole-mount IF in human heart samples

Blocks of human heart specimens (1 mm^3) harvested during routine autoscopic examination, were fixed in 1% PFA for 10–15 min, washed three times for 5 min in $1 \times \text{PBS}$, incubated for 4 consecutive days with anti-TOH primary antibody diluted in $1 \times \text{PBS}$, supplemented with 1% BSA and 2% Triton X-100, at 4°C . Samples were then incubated for 3 consecutive days with a Cy3-conjugated anti-rabbit antibody diluted in $1 \times \text{PBS}$, supplemented with 1% BSA and 0.5% Triton X-100, at 4°C . Sequential stacks of images spaced by $1.5 \mu\text{m}$ along the Z-axis were acquired using a multiphoton microscope (Scientifica 2P, Uckfield, UK) equipped with a Chameleon titanium sapphire laser (Coherent Inc., Santa Clara, CA, USA). The excitation wave-length was tuned to 1040 nm with direct detection at $535 \pm 25 \text{ nm}$. Images were analysed and rendered in 3-D, using Imaris (Bitplane, Zurich, Switzerland).

Evaluation of SN process (SNP) density

SNP density was evaluated in heart sections co-stained with anti-TOH, to detect SNs, and anti-dystrophin antibody or FITC-conjugated wheat germ agglutinin, to mark CMs, and analysed using a confocal microscope (model SP5, Leica Microsystems). For the mouse hearts, the number of TOH positive processes per CM, in the EPicardial (EPI) and ENDOcardial (ENDO) regions, was

estimated in six non-consecutive sections at the level of the heart base, the mid-portion of the ventricles and the apex. In total, six hearts were analysed.

For rats ($n = 3$ hearts) and rabbits ($n = 3$ hearts), we analysed six non-consecutive cryosections from the mid portion of the ventricles. For human hearts ($n = 1$ neonate and $n = 1$ adult), we investigated six non-consecutive sections from the mid portion of the ventricles.

Evaluation of CM cross-sectional areas

The same sections used to assess SN density were analysed to estimate the cross-sectional areas of the left ventricle (LV) EPI *vs.* ENDO CMs. Here, we acquired, using a fluorescence microscope (model DC130; Leica Microsystems) and analysed images from the mid portion of the ventricles. Neighbouring images were automatically aligned and composed using the photomerge function in Photoshop, version 8.0 (Adobe Systems Inc., San Jose, CA, USA). We restricted the analysis to CMs with the same orientation, as identified by a score higher than 0.9 in the eccentricity index. Cross-sectional areas were measured both manually using ImageJ (NIH, Bethesda, MD, USA) (Schneider *et al.*, 2012) and with an automated plugin developed in MatLab (MathWorks Inc., Natick, MA, USA). All CMs from the posterior, lateral and anterior LV wall were evaluated. Longitudinal heart cryosections were also obtained from additional subsets of normal mice, processed for IF, as described above, and used to measure the long axis of EPI and ENDO CMs.

Automated assessment of cross-sectional CM area

CM cross-sectional areas were measured in the IF images of murine heart sections from the mid-portion of the ventricles, composed of a single image as described above. The analysis uses a custom-developed plugin running in MatLab. Briefly, each cell contour is identified with image segmentation tools, and automatically assigned a unique region of interest, allowing measurement of the cell cross-section. Colour-coded maps were generated in which the cell colour corresponds to the surface area value, according to the indicated Lookup Table, thus displaying each cell with a color reflecting its size.

Tissue clarification and mesoscale imaging

Clarified heart samples were prepared by adapting the tissue clearing 'CLARITY' protocol as described previously (Chung & Deisseroth, 2013; Costantini *et al.*, 2015). Briefly, α -MyHC-ChR2 transgenic mice were anaesthetized by inhaled isoflurane (5%). Hearts were harvested and immediately cannulated and retrogradely

perfused with 4% PFA (w/v in $1 \times$ PBS) followed by hydrogel solution [4% (w/v) acrylamide, 0.05% (w/v) bisacrylamide, 0.25% (w/v) VA044 initiator]. The gel-embedded LV was extracted from the gel, dissected and incubated in the clearing solution (sodium borate buffer 200 mM, pH 8.5; 4% sodium dodecyl sulphate) at 37°C with gentle shaking. After clearing, the sample was stained first with anti-TOH antibody (dilution 1:200) for 3 days at 4°C, then with a secondary antibody conjugated with Alexa Fluor 488 (AB150077; dilution 1:100; Abcam) for 2 days at room temperature. Finally, samples were optically cleared with 2,2'-thiodiethanol (68% TDE/PBS) and imaged with a custom-made two-photon fluorescence microscope. Briefly, a mode locked Chameleon titanium sapphire laser (120 fs pulse width, 90 MHz repetition rate; Coherent Inc.) operating at 710 nm was coupled with a custom-made scanning system based on a pair of galvanometric mirrors (LSKGG4/M; Thorlabs, Newton, NJ, USA). The laser was focused on the specimen with a refractive index tunable $25 \times$ objective (LD LCI Plan-Apochromat 25x/0.8 Imm Corr DIC M27; Carl Zeiss, Oberkochen, Germany). The system was equipped with a closed-loop xy stage (U-780 PILine® XY Stage System; Physik Instrumente, Karlsruhe, Germany) for radial displacement of the sample and with a closed-loop piezoelectric stage (ND72Z2LAQ PIFOC objective scanning system, 2 mm travel range; Physik Instrumente) to shift the objective along the Z-axis. The fluorescence signal was collected via two independent GaAsP photomultiplier modules (H7422; Hamamatsu Photonics, Bridgewater Township, NJ, USA). Band-pass emission filters centered at 600 ± 26 nm and 520 ± 18 nm, respectively, were used for *td-Tomato* and Alexa Fluor 488 detection, respectively. Stacks of $450 \times 450 \mu\text{m}$, with a depth of $400 \mu\text{m}$ and a Z-step of $2 \mu\text{m}$ were acquired. To cover a larger surface area, serial Z-stacks of adjacent regions, laterally overlapped by $40 \mu\text{m}$, were collected and images of corresponding Z-planes were stitched using ZetaStitcher (<https://github.com/lens-biophotonics/ZetaStitcher>), a 3-D stitching tool specifically designed to handle very large images.

Microdissection of EPIcardial and ENDOcardial regions

The mouse LV free wall was dissected and upon removal of papillary muscles frozen in liquid nitrogen. Cryosections were cut from a $300 \mu\text{m}$ thick tissue portion of the EPI and ENDO region, and pooled separately for RNA and protein isolation. The expression level of Kv4.2 in extracts from EPI *vs.* ENDO regions was used as marker of efficient separation of the surgically dissected myocardial fragments (Fig. 2A) (Bru-Mercier *et al.*, 2003; Brunet *et al.*, 2004; Teutsch *et al.*, 2007).

ISH

ISH on paraffin-embedded mouse heart sections was performed as described previously (Ammirabile *et al.*, 2012). Images were acquired using a DMR microscope (Leica Microsystems).

Quantitative RT-PCR analysis

Total RNA was extracted from heart tissue using, the SV Total RNA Isolation System Z3100 (Promega, Madison, WI, USA), as described previously (Zaglia *et al.*, 2014). The primers used were: (GAPDH: forward: 5'-ACCATCTTCCAGGAGCGAG-3', reverse: 5'-CCTTCTCCATGGTGGTGAAGAC-3'; MuRF1: forward: 5'-ACCTGCTGGTGGAAAACATC-3', reverse: 5'-CTTCGTGTTCCCTTGCACATC-3'; Kv4.2: forward: 5'-CCTGGAGAAAACCACGAACC-3', reverse: 5'-GACTGTGACTTGATGGGCGA-3').

WB and immunoprecipitation

Protein extracts from the surgically dissected LV EPI and ENDO regions were obtained as described previously (Zaglia *et al.*, 2013). Immunoprecipitation was performed with anti-cardiac troponin I antibody (Saggini *et al.*, 1989) adsorbed on A/G agarose beads (Santa Cruz Biotechnology, Santa Cruz, CA, USA), as described previously (Bertaglia *et al.*, 2012). Precipitated proteins were revealed with anti-poly-Ubiquitin antibody (dilution 1:1000; Merck Millipore, Billerica, MA, USA).

Statistical analysis

All data are expressed as the mean \pm SEM. Comparison between the experimental groups was made using a non-paired Student's *t* test and ANOVA, with Bonferroni correction. $P < 0.05$ was considered statistically significant.

Results

Direct neuro-cardiac coupling regulates CM size, *in vitro*

We have demonstrated that SNs and CMs, in co-culture, develop in time junctional sites, where intercellular communication takes place at a restricted extracellular signalling domain. The ultrastructure and the biophysics of cardiac synapses suggest that they underlie a stable intercellular interaction (Prando *et al.*, 2018). Consistently, images of the co-cultures, acquired every 30 min, over a period of 6 h, showed that most neuronal processes, anchored to CMs, remained attached to the same cell

portion for the whole time (average interaction time: 300 min, 240–360 min, $n = 48$ SN processes). By contrast, in SN co-cultured with CFs, neuronal process/target interactions were transient and, in most cases, lasted less than 2 h (average interaction time: 90 min, 60–120 min, $n = 28$ SN processes) (Fig. 1A and B). Given our previous demonstration that SNs modulate CM proteostasis and size (Zaglia *et al.*, 2013), such evidence suggests that innervated CMs would receive more trophic inputs (thus becoming larger) than the non-innervated ones. This was confirmed by morphometric analysis of the cultured cells showing selective enlargement of innervated CMs, compared to the non-innervated ones (CM area, innervated CMs: 1197.03 ± 84.46 vs. non-innervated CMs: $844.47 \pm 59.38 \mu\text{m}^2$) (Fig. 1C and D). Nicotine treatment, which was used to enhance SN activity, did not affect the size of CM cultured alone (CM area, basal conditions: 819.29 ± 66.06 vs. nicotine-treated CMs: $669.53 \pm 61.40 \mu\text{m}^2$). These results demonstrate that direct contact has a role in neuro-cardiac communication, both in the acute activation of adrenergic responses (Prando *et al.*, 2018) and in the regulation of CM structure, occurring over the long term. When translated to the intact heart, which is heterogeneously innervated by SNs, a correlation between local innervation density and CM size could be inferred. To establish such hypothesis, we compared the size of CMs from differently innervated regions in both rodent and human myocardium.

Heterogeneous CM size throughout the myocardium reflects SN distribution

It is well accepted that CM orientation varies across the LV wall, with the cellular long axis rotating of $\sim 180^\circ$ from the outer to the inner side (Healy *et al.*, 2011) and, based on the fibre orientation, three adjacent layers, namely the sub-EPIcardium (EPI), mid-myocardium (MID) and sub-ENDOcardium (ENDO), can be identified. In transverse mouse heart sections, similarly oriented CMs were found within the 20–25 cell layers underneath the epicardium and the innermost 20–25 layers (ENDO) embraced by the papillary muscle basis and the MID. Cells belonging to these two regions had an eccentricity index >0.9 , indicating that they had parallel orientation. It has previously been demonstrated that, in the mouse heart, the EPI is more densely innervated than the ENDO (Chen *et al.*, 2007) and in line with this, increased TOH protein content was detected in the former, when WB was performed on extracts from the two surgically dissected regions (Fig. 2A and B). Consistently, quantification of the number of TOH positive fibres per CM revealed that the EPI cells were almost three-fold more innervated than the ENDO ones (Fig. 2C). Together with our published evidence (Zaglia *et al.*, 2013) and the results obtained in

co-cultures (see above), these data prompted us to assess whether CMs from the highly innervated EPI region were larger than those of the ENDO. We thus measured the cross-sectional area of CMs, stained with an antibody to dystrophin, in the EPI and ENDO regions of the posterior, lateral and anterior LV walls. The results of these analyses showed that, for each heart region, CM size paralleled the local neuronal density and that, on average, EPI CMs were between 1.5- and 2-fold larger than the less

innervated ENDO cells (Fig. 2C, E and F). Despite these differences, the long-axis length distribution was identical in cells from all aforementioned regions (Fig. 2D). Given that the intra-myocardial displacement of sympathetic nerves varies among mammals, we aimed to assess the SN density/CM size relationship in hearts from rodents (i.e. rat, rabbit) and humans.

For the human heart, in the present study, we analysed specimens from one heart of a neonate who died as a

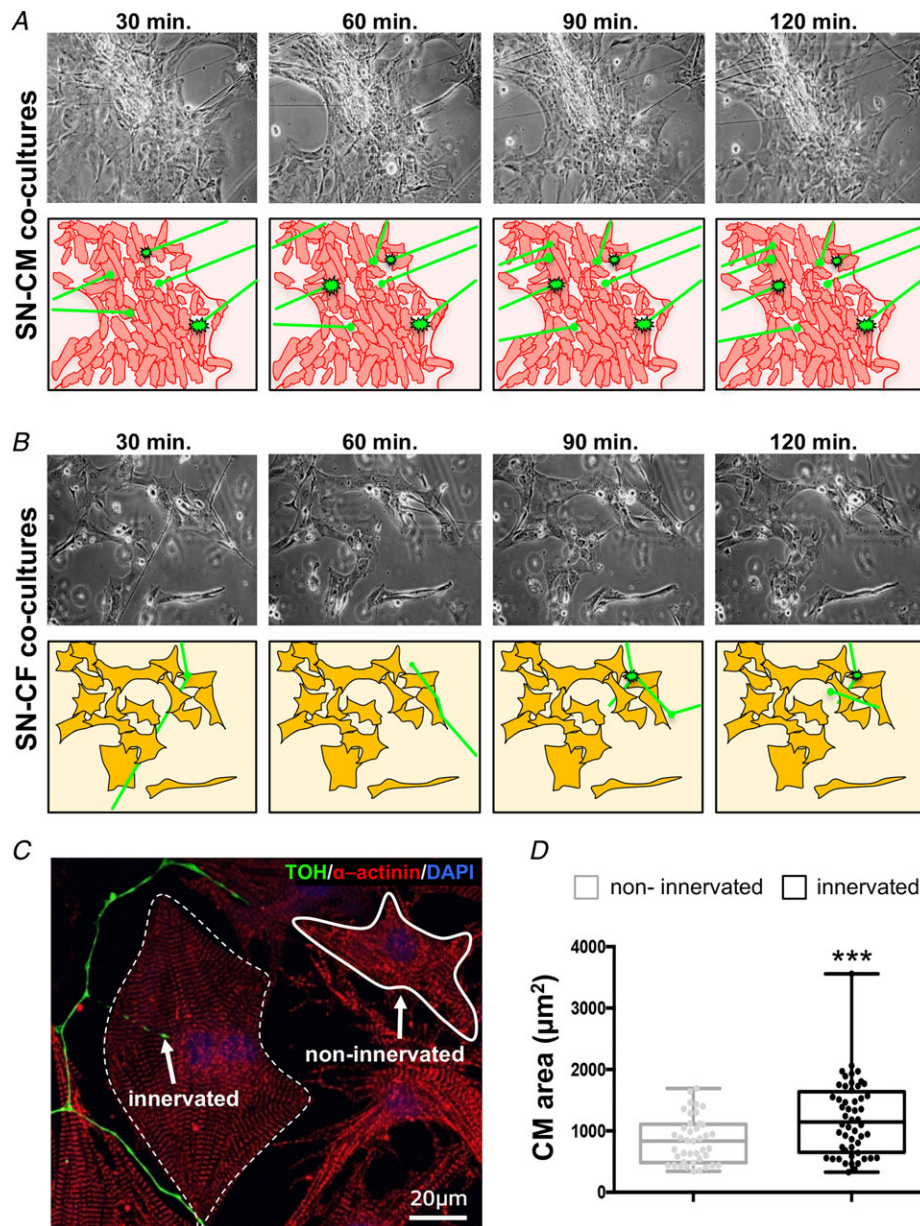


Figure 1. Long-term effects of sympathetic neurons on cardiomyocyte size

A, time course of SN-CM contacts in co-cultures. B, time course of SN-CF contacts in co-cultures. Bottom: representative cartoons. C, IF analysis on 15-day SN-CM co-cultures co-stained with antibodies to TOH and sarcomeric actinin (α -actinin). Nuclei were counterstained with 4',6-diamidino-2-phenylindole. D, area of non-innervated vs. innervated CMs. Bars indicate the SD ($n = 42$ and 53 CMs, respectively; $***P < 0.001$). [Colour figure can be viewed at wileyonlinelibrary.com]

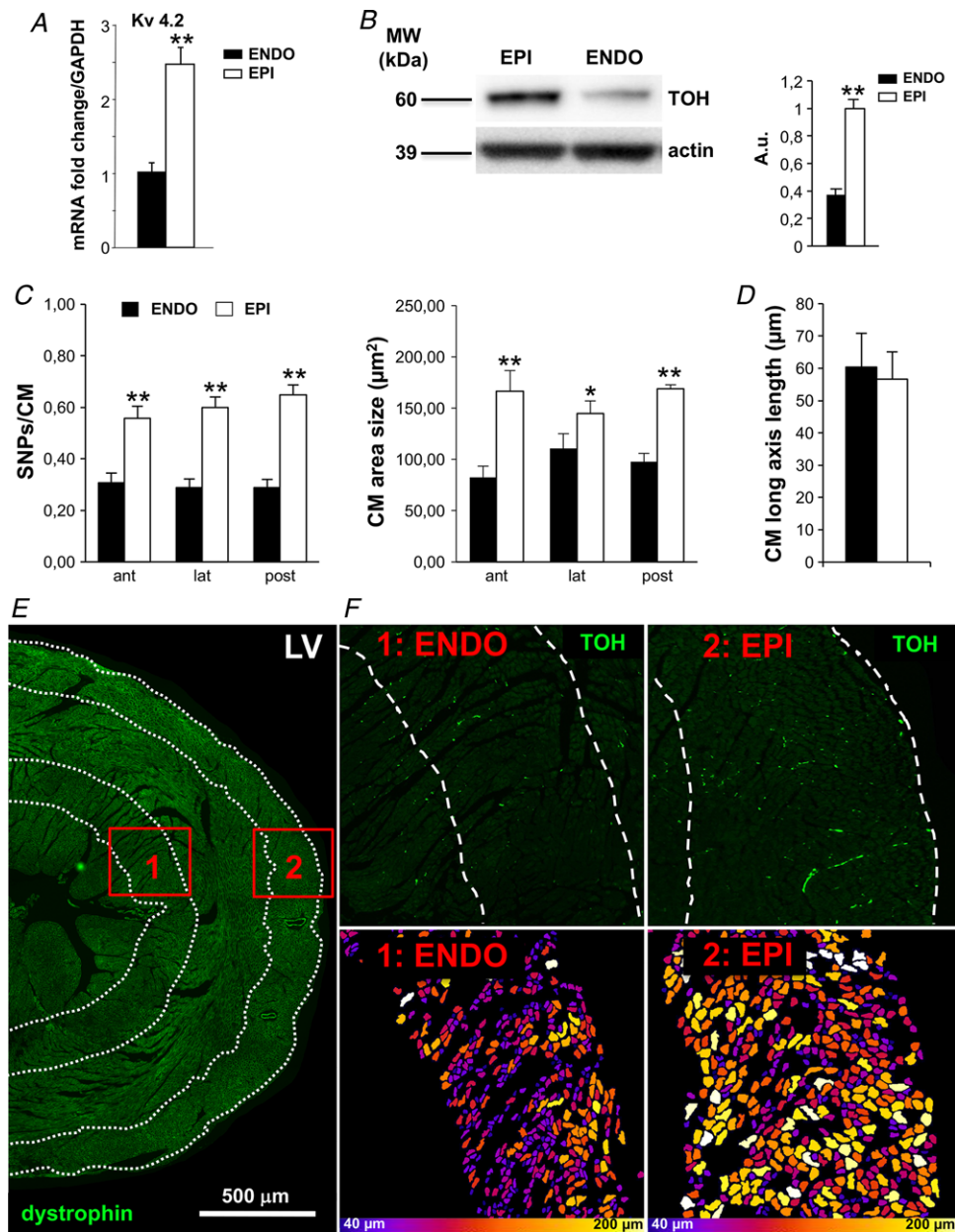


Figure 2. Correlation between the topology of the sympathetic neuron network and cardiomyocyte size distribution in the adult murine heart

A, Kv4.2 expression, as evaluated by a quantitative RT-PCR, on extracts from surgically dissected EPI and ENDO regions of wild-type mouse hearts. The expression of Kv4.2 was used to assess the efficacy of EPI vs. ENDO surgical dissection (see Methods) ($n = 6$ hearts for each group; $**P < 0.01$). **B**, protein content of TOH, as measured by WB in extracts from the EPI and ENDO regions of the LV wall. Staining with an antibody to actin was used to ensure equal protein loading (left). Right: relative densitometry normalized for the immunoreactivity of the EPI sample. Error bars indicate the SEM ($n = 3$ hearts, $**P < 0.01$). **C**, SNP density (normalized to CM number), evaluated in the ENDO (black bars) and EPI (white bars) regions from the anterior, lateral and posterior LV wall of mouse heart (left). In the same myocardial regions, CM cross-sectional areas were evaluated (right). Error bars indicate the SEM ($n = 8$ hearts for each group; $*P < 0.05$; $**P < 0.01$). **D**, evaluation of the CM length in the EPI vs. ENDO regions of the LV wall. Error bars indicate the SEM ($n = 3000$ CMs for each group, evaluated in six hearts). **E**, LV section of a mouse heart stained with an antibody to dystrophin. The dashed lines delineate the ENDO and EPI regions analysed. **F**, enlargements of the areas enclosed in the red boxes in (**E**), from the consecutive serial section. Top: SNs in the ENDO (left) and EPI (right) regions, stained with an antibody to TOH. Bottom: pseudocolour scale map (see Methods) obtained from dystrophin staining, highlighting the differences in the single cell cross-sectional areas in the same ENDO and EPI regions. [Colour figure can be viewed at wileyonlinelibrary.com]

result of extracardiac causes. In detail, we analysed six non-consecutive sections, from the mid-portion of the ventricles and compared the EPI and ENDO SN density and CM size of corresponding regions. Although the low statistical power did not allow proper quantitation, this analysis was in line with the correlation between SN density and CM size distribution demonstrated for rodent hearts: (i) anterior LV: SN/CM ratio: EPI, 0.045 ± 0.005 vs. ENDO, 0.077 ± 0.006 ; CM cross-sectional areas: EPI, 22.50 ± 2.82 vs. ENDO, $41.79 \pm 3.05 \mu\text{m}^2$; (ii) lateral LV: SN/CM ratio: EPI, 0.040 ± 0.004 vs. ENDO, 0.070 ± 0.007 ; CM cross-sectional areas: EPI, 23.99 ± 0.69 vs. ENDO, $47.08 \pm 3.02 \mu\text{m}^2$; and (iii) posterior LV: SN/CM ratio: EPI, 0.040 ± 0.004 vs. ENDO, 0.060 ± 0.005 ; CM cross-sectional areas: EPI, 33.06 ± 2.77 vs. ENDO, $47.42 \pm 3.33 \mu\text{m}^2$.

Our results demonstrate that the SN density/CM size correlation holds true in the hearts from all species analysed, regardless of the species-specific innervation pattern (Fig. 3).

3-D reconstruction of the SN network in the murine and human myocardium

Given the complex architecture of the neuronal network, the tortuosity and the multiple directions of intra-myocardial processes, the inspection of single thin tissue sections fails to inform on the actual displacement of the neurons throughout the heart walls. This leaves the impression that, among similarly sized CMs, in the same field of view, some are innervated, whereas others are not. Such anatomy would hardly sustain a model where neuronal input to CMs is confined to the cells in direct contact.

To finely describe the intra-myocardial neuronal network, we thus aimed at visualizing heart innervation in 3-D using whole-mount IF in tissue-clarified LV blocks (Fig. 4). Neurons were stained with anti-TOH antibody in a α -MyHC/ChR2-*tdTomato* mouse heart, which natively expresses membrane tethered red fluorescent *tdTomato*. The tissue volume was reconstructed by combining overlapping Z-stacks, acquired with a two-photon microscope. This allowed 3-D mesoscale reconstruction of the SN network within its intact anatomical context (Fig. 4A–D). Quantitative analysis of the interaction between SNs and CMs across the LV wall showed that CMs in the EPI were contacted on average by more neuronal processes than those in the ENDO region (EPI: 1.69 ± 0.10 vs. ENDO: 1.24 ± 0.08 , in neuronal processes per cell) (Fig. 4D and E). These results revealed two important concepts: (i) as the entire CMs volume is accounted for, almost all CM in the heart wall are innervated and (ii) the higher neuronal density observed in the EPI vs. ENDO, when assessed in thin sections, depends on the greater branching of the neurons in the former region. Given the regular

displacement of varicosities along the processes, and the local nature of intercellular communication at the NCJ, such an arrangement implies that CMs in the different heart regions would receive heterogeneous trophic input, thus explaining the SN density/CM size relationship.

To determine as a proof-of-concept whether the myocardial innervation architecture shows a similar complexity in humans, we sampled myocardial blocks from the EPI region of a post-mortem heart and performed whole-mount IF with anti-TOH antibody. Interestingly, neurons were highly arborized, resulting in multiple interconnected processes displaying regularly distributed varicosities, which appeared to envelop dark volumes that, with respect to their autofluorescence, geometry and size, are suggestive of CMs (Fig. 5).

Establishment and maintenance of regional differences in CM size depends on neurogenic signalling

To understand whether neurons have a causal role in shaping the myocardial architecture, we interfered, by pharmacological or genetic means, with the signalling pathway relaying the neuronal effects on CM proteolysis and cell size. Accordingly, we first assessed the CM cross-sectional area in the LV wall during the early post-natal weeks, when cardiac sympathetic innervation is established. At P1, when the heart is still denervated, the ratio between EPI and ENDO CM area is ~ 1 , indicating that, in the absence of neurons, similarly oriented CMs have the same size distribution. One week after birth, as neurons appear at the epicardial front, EPI CMs enlarge more than the ENDO ones, and such a difference progressively increases in time and stabilizes only when heart innervation is completed (~ 3 weeks) (Kimura *et al.*, 2012; Kreipke & Birren, 2015) (Fig. 6A and B). Interestingly, early pharmacological neuronal ablation, when performed before the development of cardiac innervation (see Methods), caused heart atrophy, and did not allow EPI/ENDO heterogeneity in CM size to be established (Fig. 6B).

A disappearance of such physiological transmural differences in size was also observed when adult normally innervated hearts underwent the same treatment for SN ablation, which resulted in overall heart atrophy (HW/BW, control: 4.3 ± 0.3 vs. denervated: $3.8 \pm 0.4 \text{ mg g}^{-1}$), mostly affecting cells of the EPI region (Fig. 6C and D). Of note, other conditions promoting heart atrophy, such as caloric restriction (HW/BW, caloric restriction: $3.9 \pm 0.2 \text{ mg g}^{-1}$), resulted in similar fractional decrease in size of both EPI and ENDO cells (Fig. 6C and D), and thus did not affect transmural cell size heterogeneity.

The evidence that regional tuning of cell growth in the postnatal development parallels the appearance of

cardiac SNs, together with the effect of neuronal removal in the adult heart, indicates that neurogenic inputs are required for both establishing and maintaining correct myocardial architecture. To address whether such effects depended on the neuronal modulation of CM proteolysis (Zaglia *et al.*, 2013), we interfered with the β 2-AR/MuRF1 signalling axis without perturbing heart innervation. We first analysed hearts of normal adult mice upon systemic delivery of β 2-AR modulating drugs, with the rationale

that they would act diffusely on the heart irrespective of the neuronal topology. Treatment with the β 2-AR antagonist ICI-118-551, which interfered (to the same extent in all CMs) with activation of β 2-AR, resulted in cardiac atrophic remodelling (HW/BW, control: 4.3 ± 0.3 vs. ICI-118551: 4.0 ± 0.1 mg g⁻¹), which was predominant in the highly innervated (hence more stimulated) EPI regions, therefore reducing the differences in cell size between EPI and ENDO (Fig. 6C and E). Conversely,

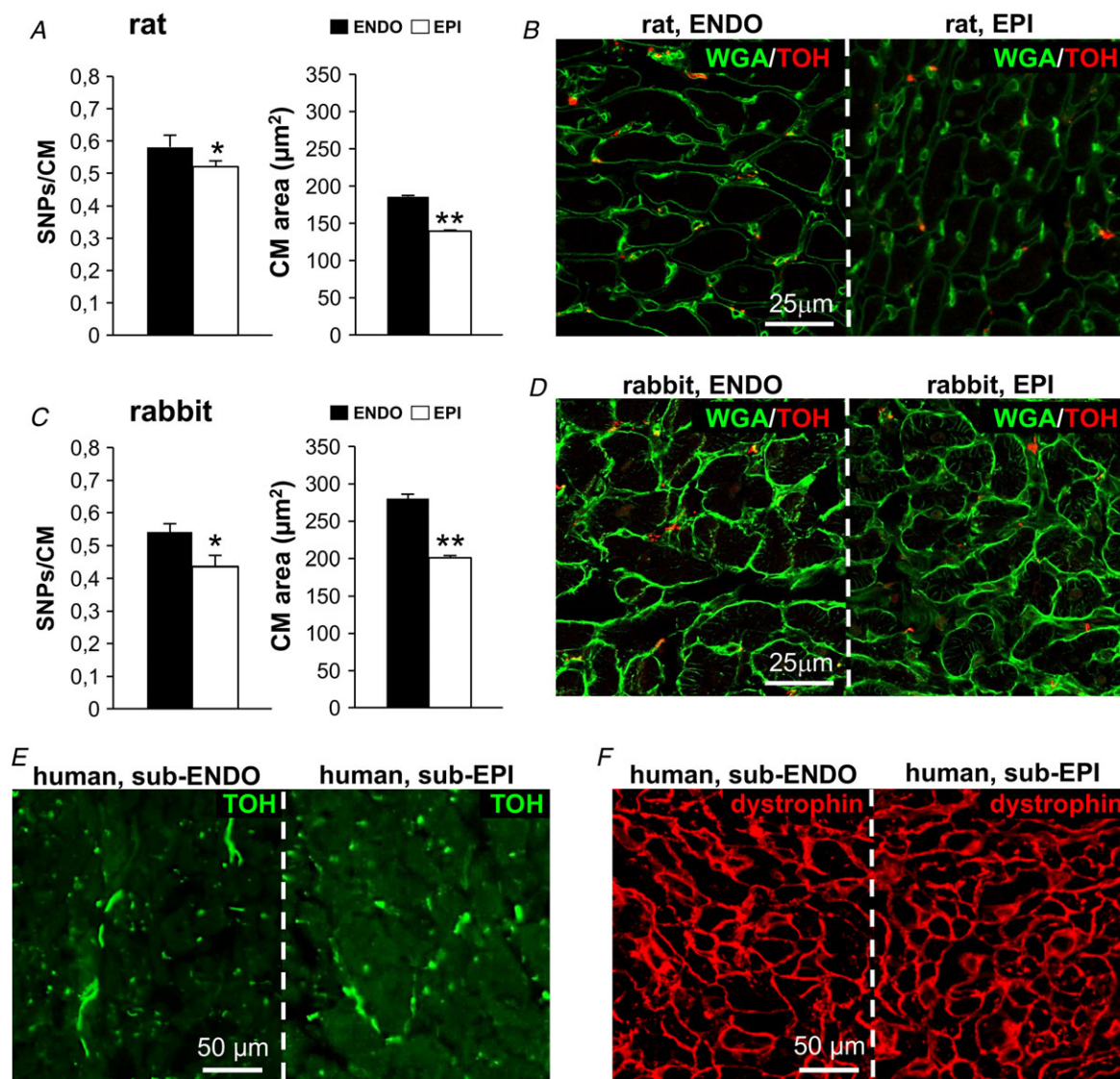


Figure 3. Correlation between the topology of the sympathetic neuron network and cardiomyocyte size distribution in the rodent and human myocardium

A and C, ratio between sympathetic neuron processes (SNPs) and CMs, evaluated in the ENDO (black bars) and EPI (white bars) regions from the LV wall of the rat (A, left) and rabbit (C, left) hearts. CM cross-sectional areas were evaluated in the same regions (A and C, right). Error bars indicate the SEM ($n = 3$ hearts for each group; $*P < 0.05$; $**P < 0.01$). B and D, confocal IF analysis on LV sections from rats (B) and rabbits (D), co-stained with an antibody to TOH and FITC-conjugated wheat germ agglutinin (WGA). Images are details from EPI and ENDO regions. E and F, confocal IF analysis of human post-mortem neonatal heart specimens, sectioned serially and stained with either an antibody to TOH (left, green signals) or anti-dystrophin (right, red signals). [Colour figure can be viewed at wileyonlinelibrary.com]

the β 2-AR agonist, clenbuterol, caused heart hypertrophy (HW/BW, control: 4.5 ± 0.2 vs. clenbuterol: 5.5 ± 0.3 mg g⁻¹) to a higher extent in the ENDO CMs, which grew larger (i.e. area was two-fold that of the EPI CMs), probably because they were super-sensitive to the β 2-AR agonist, thus reversing the pattern of CM size heterogeneity (Fig. 6F and G). Finally, because β 2-ARs operate on cell size by modulating the ubiquitin ligase MuRF1, we expected that, in the absence of MuRF1, regional differences would not be detected. In line with our hypothesis, MuRF1 KO hearts, which did not show alterations in sympathetic innervation, displayed hypertrophic remodelling of both the ENDO and EPI CMs, which measured approximately the same size (HW/BW,

control: 4.7 ± 0.5 vs. MuRF1 KO: 5.3 ± 0.3 mg g⁻¹) (Fig. 6F and H).

Local control of CM proteostasis by SNs

Collectively, the cell-selective neuro-cardiac communication (Prando *et al.*, 2018) and the evidence that the highly innervated EPI CMs enlarge more than the ENDO cells via the β 2-AR/MuRF1 axis, prompted us to infer that the more pronounced remodelling of the former, upon denervation (Fig. 6D), resulted from higher activation of the atrophic programme. Accordingly, we used ISH in adult heart sections to assess the expression pattern of MuRF1 upon cardiac denervation. In line with

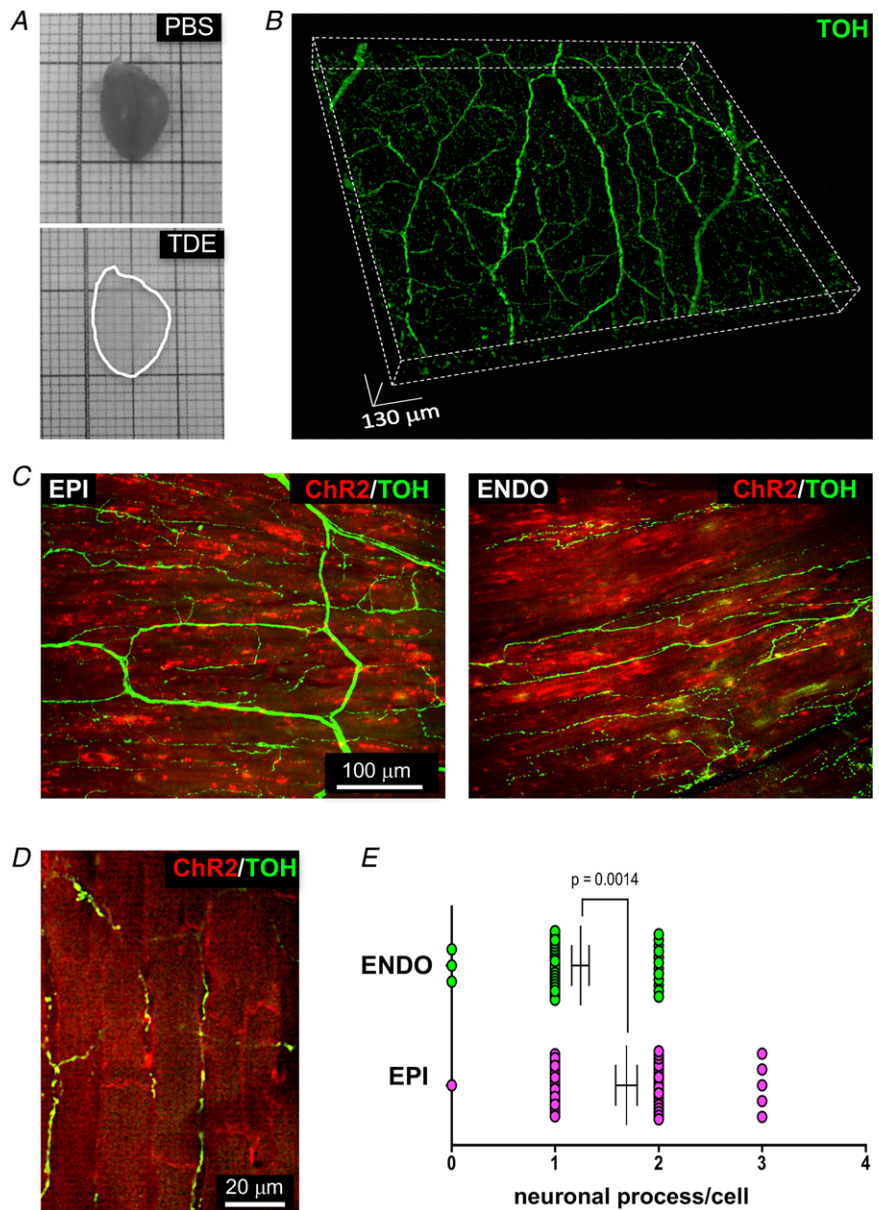


Figure 4. 3-D imaging of the neuronal network in the murine myocardium
 A, images of whole left ventricle before (top) and after tissue clearing (bottom). B, 3-D rendering of the SN network imaged upon whole-mount IF, with an antibody to TOH, in a tissue-clarified LV block. C, maximum intensity projection of multiphoton image stacks acquired along 400 μ m in tissue clarified LV blocks from the EPI and ENDO regions of the LV of a α -MyHC-ChR2 mouse heart, stained with anti-TOH antibody. D, representative single optical section of a sample processed as in (C), illustrating the spatial resolution resolving the neuro-cardiac interactions, obtained in the clarified myocardial blocks with two-photon imaging, and used for quantification of neuronal processes/cell (E) in EPI (45 CMs, magenta) and ENDO (45 CMs, cyan) regions. [Colour figure can be viewed at wileyonlinelibrary.com]

our hypothesis, 1 day after 6-OH-DA injection, MuRF1 expression was higher in the EPI (Fig. 7A and B) than in the ENDO. Molecular and biochemical analyses of myocardial extracts from surgically dissected EPI vs. ENDO regions confirmed that the expression level of MuRF1 was higher in the outer heart layers and was consistently accompanied by increased ubiquitination of the MuRF1 sarcomeric target, cardiac TnI (Fig. 7C and D).

Altogether, our results indicate that the direct neuro-cardiac communication takes place *in vivo* and, although this finely regulates heart rate in the SAN (Prando *et al.*, 2018), it shapes myocardial architecture in the ventricles via constitutive cell-targeted modulation of the CM proteolytic machinery.

Discussion

The muscular component of the heart walls is made of multiple consecutive layers of interconnected CMs, which show, from the inner to the outer wall sides, a differing size and orientation, as well as a distinctive ion channel expression profile (Antzelevitch *et al.*, 1991; Honen & Saint, 2002; Strom *et al.*, 2010; Qu & Robinson, 2004; Kreipke & Birren, 2015). Such a construction is tailored to achieve optimal efficiency of the pump and resistance to mechanical stretch generated by cardiac activity. Although several physiological (e.g. exercise, pregnancy) and pathological (e.g. hypertension, aortic stenosis) conditions are known to modulate CM size via mechanical, metabolic and neuro-hormonal inputs, hypertrophic growth of the heart does not alter the steady wall geometry, which remains unchanged throughout life. We have previously shown that cardiac SNs provide constitutive trophic input to CMs, which is mediated by β 2-AR-dependent control of the balance between protein synthesis and degradation, operated by the ubiquitin/proteasome system and autophagy/lysosome system (Zaglia *et al.*, 2013). More recently, we have

demonstrated that SNs establish stable contacts with CMs, restricting neuro-cardiac signalling to the directly innervated cells. Furthermore, cardiac SNs distribute within the heart walls with a non-random pattern, and different heart regions are therefore heterogeneously innervated. All of these concepts coalesce in the results of the present study, which demonstrates how the physiological geometry of myocardial walls is shaped by the topology of the cardiac sympathetic network via local modulation of the CM proteolytic machinery.

We have recently addressed the physiology of sympatho-cardiac communication *in vivo*, by exploiting the capability of optogenetics to non-invasively control neuronal activity, using a transgenic mouse expressing ChR2 selectively in SNs. Combination of optical actuation with electrophysiological, pharmacological and morphological assays demonstrated that SNs finely and efficiently regulate heart rate as a result of the establishment of junctional sites with SAN CMs, allowing intercellular communication to occur in a synaptic fashion (Prando *et al.*, 2018). Although the structural and ultrastructural features of neuro-cardiac interaction in the ventricles suggest that such a modality of communication may also underlie the neurogenic control of contractility, this hypothesis is not easily addressable *in vivo*. To test whether neurons communicate to ventricular CMs locally, we exploited the effect of SNs on CM size, which we previously demonstrated to depend on β 2-AR regulation of the heart cell proteostasis, as a surrogate readout of neuro-cardiac coupling. The density of the neuronal processes or the total axonal length/tissue volume have previously been used to infer the degree of sympathetic activation of the target tissue (Cao *et al.*, 2000; Li *et al.*, 2004; Ieda *et al.*, 2007). Our finding that the regional density of SNs positively correlates with CM size supports the model where the effect of SNs is confined to the cells in their immediate surroundings. This is further corroborated by the evidence that transmural

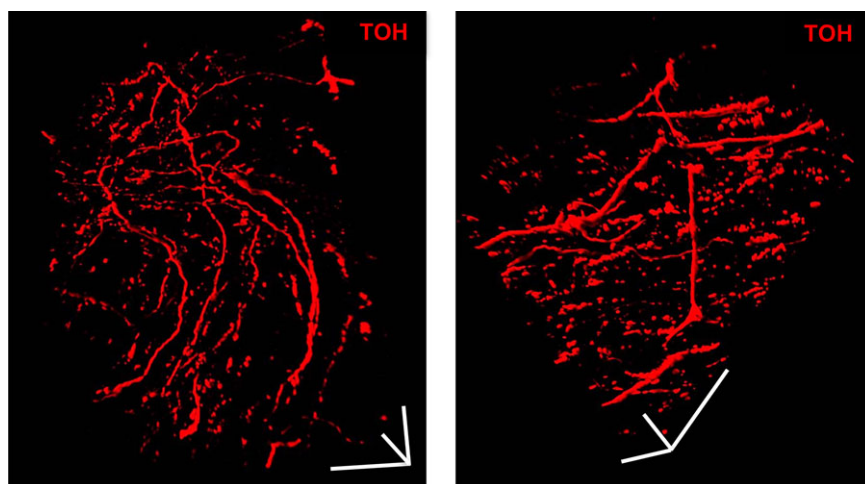


Figure 5. 3-D imaging of the neuronal network in the human myocardium

Topology of the SN network, reconstructed with 3-D rendering of 600 images acquired with a multiphoton microscope along 200 μ m, upon whole mount IF in 1 mm³ LV blocks from the EPI region, stained with anti-TOH antibody. Images were acquired with an 18 \times objective, 1.1 NA, allowing a large field of view (850 \times 850 μ m) at high resolution. Image series were acquired along the Z-axis, with a step size of 1.5 μ m and processed and analysed with a software for 3-D rendering (Imaris). [Colour figure can be viewed at wileyonlinelibrary.com]

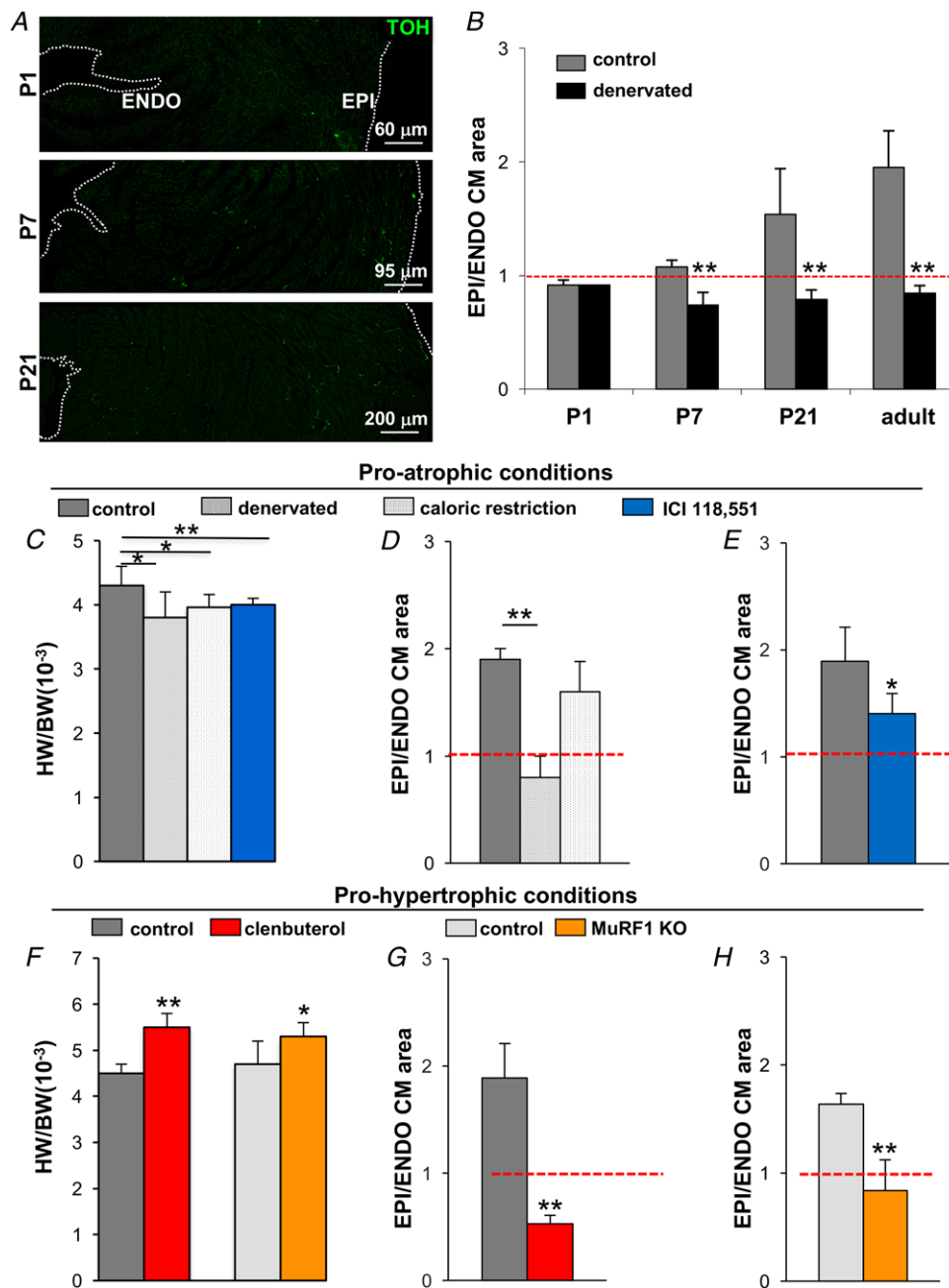


Figure 6. Sympathetic innervation is required to establish and maintain the transmural heterogeneity in cardiomyocyte size

A, IF analysis of heart sections from P1, P7 and P21 mice stained with an antibody to TOH. Images are details of the LV lateral wall. The dashed lines indicate the endocardial and the epicardial layers. B, D, E, G and H, ratio between the cross-sectional areas of EPI vs. ENDO CMs, analysed in (B) heart sections from P1, P7, P21 and 3-month-old control and denervated mice; (D) untreated controls vs. denervated mice vs. mice undergone caloric restriction; (E and G) untreated controls vs. mice treated systemically with the β 2-AR antagonist ICI 118,551 (E) or the β 2-AR agonist clenbuterol (G); (H) controls vs. MuRF1 KO mice. C and F, heart weight/body weight (HW/BW) relative to the experimental groups in (D), (E), (G) and (H). In all graphs, bars indicate the SEM (all CMs of the anterior, lateral and posterior regions of the LV wall were measured, $n = 6$ hearts for each group; * $P < 0.05$, ** $P < 0.01$). [Colour figure can be viewed at wileyonlinelibrary.com]

heterogeneity in cell size disappears upon neuronal removal and does not establish whether heart innervation is prevented, and is also ablated when innervation anatomy is by-passed by the systemic addition of adrenergic agonists (Fig. 6). Given that workload, in addition to neuro-hormonal regulation, is a well appreciated factor affecting CM size, it could be argued that the EPI vs. ENDO differences reflect the differential action of mechanical forces in the two regions. If this were the case, because sub-endocardial layers are subjected to the highest active and passive pressures (Hoffman, 1987), ENDO CMs would be larger than the EPI ones in all mammalian hearts, independent of the innervation pattern. In addition,

cell size heterogeneity would be maintained upon sympathectomy, which, under basal conditions, does not affect workload distribution and myocardial strain (Zaglia *et al.*, 2013). Thus, our *in vitro* and *ex vivo* data support the notion that, in analogy to the mechanism warranting acute control of SAN function, the long-term effect of SNs on ventricular CM trophism is also operated locally.

The overall sympathetic network topology, as delineated in the present study by multiphoton imaging of whole-mount IF, is in good agreement with that previously described in transgenic hearts with SN expression of EGFP by Freeman *et al.* (2014). Although such a study focused on the sub-epicardial LV layers, and investigation

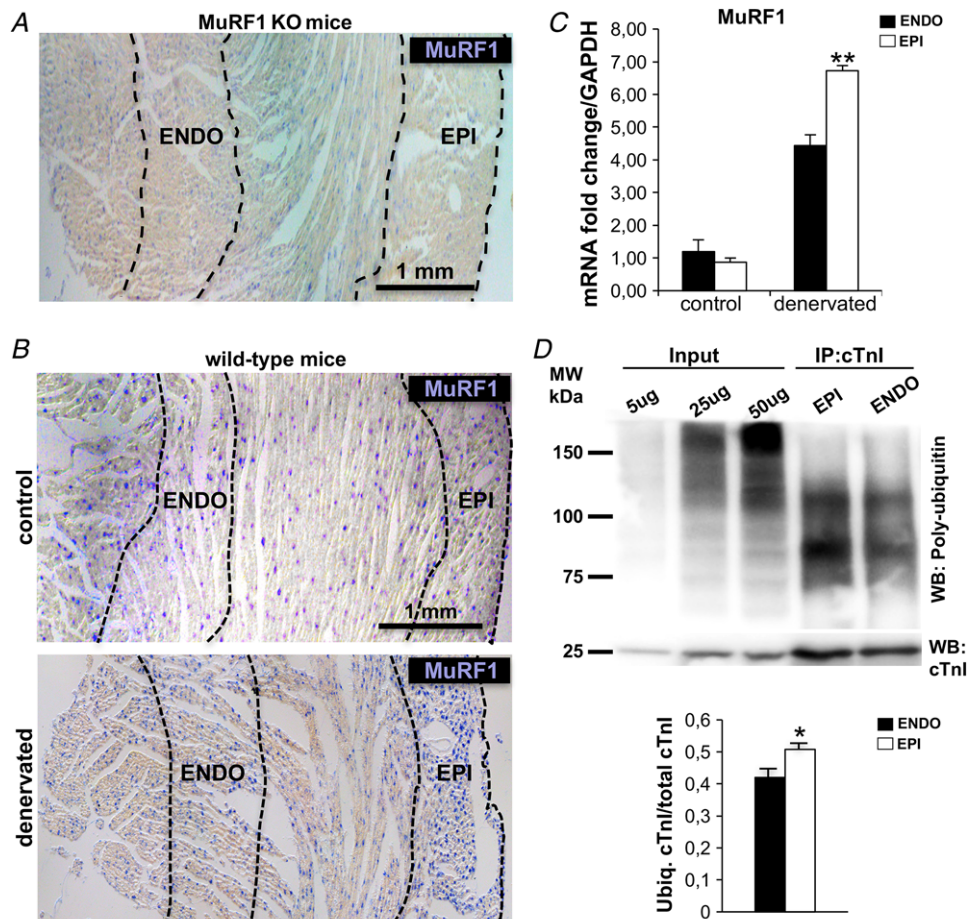


Figure 7. Regional control of cardiomyocyte MuRF1 expression by innervating neurons in the adult murine myocardium

A, ISH for MuRF1 on heart sections from MuRF1 KO mice, as a control of the probe specificity. A detail of the LV lateral wall is shown. The black lines highlight the endocardial and epicardial layers. **B**, ISH for MuRF1 on heart sections from normal and denervated wild-type adult mice. Images are details of the LV lateral wall. Dashed lines enclose the reference EPI and ENDO regions. **C**, MuRF1 expression as evaluated by a quantitative RT-PCR on extracts from surgically dissected EPI and ENDO regions of normal vs. denervated wild-type hearts. Bars indicate the SEM ($n = 6$ samples for each group; $**P < 0.01$). **D**, immunoprecipitation with an anti-cardiac troponin I (cTnI) antibody on protein extracts from ENDO and EPI regions of denervated mouse hearts. Immunoprecipitated extracts were blotted for poly-ubiquitin and the total amount of cTnI was used as a normalization control. Input represent total protein extracts. Experimental groups consisted in pooled EPI and ENDO extracts from $n = 12$ hearts. The experiments were repeated three times. Bars indicate the SEM ($*P < 0.05$). [Colour figure can be viewed at wileyonlinelibrary.com]

was limited to the tissue layers in the first 50 μm from the heart surface, the 3-D reconstruction of axonal trajectories, branching and orientation was analysed in detail, yielding information on the general topology of the cardiac sympathetic tree. Thick epicardial nerve bundles running over the epicardial surface, such as those evident in our images (Fig. 4C), turn to invade the myocardial wall and branch at variable transmural depth into thinner processes, mostly laying with an orientation parallel to the CM long axis. As a result, several thin axonal segments, often interconnected by orthogonal portions, extend parallel to each other in the interstitial space between CMs at different tissue depths (Freeman *et al.*, 2014) (Fig. 4C and D), showing the typical enlargements (i.e. varicosities) of SNs. The combination of tissue clarification and multiphoton inspection allowed us to determine the interaction between neuronal varicosities and cardiac cells across a deeper portion of intact myocardium, devoid of sectioning or processing artefacts (Cao *et al.*, 2000; Li *et al.*, 2004; Ieda *et al.*, 2007; Muhlfeld, 2010; Yokoyama & Lee, 2017). Furthermore, imaging of a large surface area of the specimen, from corresponding epicardial and endocardial sides, was used to quantitate sympathetic innervation in the respective regions. Interestingly, segmentation of the analysis on single myocardial cells showed that each CM may be in contact with multiple varicosities, from the same or different neuronal processes, which typically encompass more than one cell. This is in accordance with the interpretation that such displacement of neurons would enable co-ordinated signalling to multiple cells in laterally adjoining regions. Remarkably, although we found only rare CMs lacking neuronal contacts, the larger EPI CMs interacted, on average, with more processes than the smaller ENDO ones, suggesting that cell size may reflect the cumulative neuronal input received by a given cell in the tissue. Whether trophic neuronal signalling to CM is accomplished solely at the NCJ, and how the activation of a limited portion of the CM membrane results in the regulation of a cell-wide effect, is beyond the scope of the present study and remains to be determined. Given that CMs normally have two/three nuclei localized distally from the cell membrane, transcriptional effects, including the regulation of atrogenes (e.g. MuRF1), are probably not operated as they are in skeletal myocytes via selective signalling from the neuromuscular junction to the nearest myofibre nucleus (Gramolini *et al.*, 1997; Schaeffer *et al.*, 2001).

The molecular and biophysical mechanisms underlying the in-cell integration of multiple neuronal inputs are currently unresolved, and will be investigated in future research. When applied to the physiology of neurogenic β -AR/cAMP signalling, however, the unequivocal finding that, in the intact myocardial tissue, neurotransmitter releasing sites in SNs are quite regularly

spaced along the CM membrane merits some speculation. Research supporting the existence of neuro-cardiac synapses has revealed that the molecular elements of the β -AR/cAMP/protein kinase A (PKA) signalling pathway are tethered to the CM post-junctional membrane in correspondence with the neuronal varicosity/CM interface (Shcherbakova *et al.*, 2007). In addition, our data showed that active SNs function as point-sources of NE, which consistently activate cAMP generation from the corresponding junctional membrane portion. Previously, it was reported that free diffusion of cAMP in the cellular matrix is restricted both through degradation by phosphodiesterases (Jurevicius & Fischmeister, 1996; Perry *et al.*, 2002; Zaccolo & Pozzan, 2002; Mongillo *et al.*, 2004), as well as by physical barriers created by the tortuous CM ultrastructure, including the positioning of mitochondria and sarcomeres (Agarwal *et al.*, 2016; Richards *et al.*, 2016). The obvious implication of confined subcellular cAMP signalling is that rapid and simultaneous cAMP/PKA-dependent effects (e.g. 'inotropic' phosphorylation of sarcomeric targets such as TnI) would hardly be achieved in the entire CM volume by spatially limited second messenger domains. Remarkably, the regular extracellular displacement of release zones (as shown in the present study) at extracellular sites mirroring the regular and 'modular' CM cytoarchitecture (sarcomere Z-Z repeats, SR, T-tubuli) would provide the foundation for simultaneous activation of multiple localized pools of β -ARs upon neuronal NE discharge. Such an arrangement would overcome the need for intracellular diffusion of cAMP or its voluminous downstream effectors (i.e. PKA) over a long distance, at the same time as allowing precise signalling control, fast on-off kinetics and minimal energy expenditure, all of which are desirable properties in the sympathetic control of heart.

The data obtained in the present study offer a new viewpoint on cardiac physiology, showing the effect of sympathetic innervation on the structural modulation of the otherwise homogenous myocardium. Given that alterations in the topology of cardiac sympathetic innervation have been recognized in the pathophysiology of ageing (Myles *et al.*, 2012) and are common features of several cardiovascular disorders, associated with either heart dysinnervation (e.g. heart failure, diabetes) or denervation (e.g. heart transplantation), our results will potentially have implications for cardiovascular pharmacology and pathophysiology.

In conclusion, although the 'heart' shape is widely recognized as an icon of affection and romantic love, in the present study we demonstrate that autonomic neurons (in the metaphor, descending from the brain, emblem of rationalism and thoughtful feelings) regulate the structure of its basic components and thereby its size and architecture.

References

- Agarwal SR, Clancy CE & Harvey RD (2016). Mechanisms restricting diffusion of intracellular cAMP. *Sci Rep* **6**, 19577.
- Ammirabile G, Tessari A, Pignataro V, Szumska D, Sutura Sardo F, Benes J, Jr., Balistreri M, Bhattacharya S, Sedmera D & Campione M (2012). Pitx2 confers left morphological, molecular, and functional identity to the sinus venosus myocardium. *Cardiovasc Res* **93**, 291–301.
- Antzelevitch C, Sicouri S, Litovsky SH, Lukas A, Krishnan SC, Di Diego JM, Gintant GA & Liu DW (1991). Heterogeneity within the ventricular wall. Electrophysiology and pharmacology of epicardial, endocardial, and M cells. *Circ Res* **69**, 1427–1449.
- Bers DM & Despa S (2009). Na/K-ATPase—an integral player in the adrenergic fight-or-flight response. *Trends Cardiovasc Med* **19**, 111–118.
- Bertaglia E, Coletto L & Sandri M (2012). Posttranslational modifications control FoxO3 activity during denervation. *Am J Physiol Cell Physiol* **302**, C587–C596.
- Bru-Mercier G, Deroubaix E, Capuano V, Ruchon Y, Rucker-Martin C, Coulombe A & Renaud JF (2003). Expression of heart K⁺ channels in adrenalectomized and catecholamine-depleted reserpine-treated rats. *J Mol Cell Cardiol* **35**, 153–163.
- Brunet S, Aimond F, Li H, Guo W, Eldstrom J, Fedida D, Yamada KA & Nerbonne JM (2004). Heterogeneous expression of repolarizing, voltage-gated K⁺ currents in adult mouse ventricles. *J Physiol* **559**, 103–120.
- Cao JM, Fishbein MC, Han JB, Lai WW, Lai AC, Wu TJ, Czer L, Wolf PL, Denton TA, Shintaku IP, Chen PS & Chen LS (2000). Relationship between regional cardiac hyperinnervation and ventricular arrhythmia. *Circulation* **101**, 1960–1969.
- Chen LS, Zhou S, Fishbein MC & Chen PS (2007). New perspectives on the role of autonomic nervous system in the genesis of arrhythmias. *J Cardiovasc Electrophysiol* **18**, 123–127.
- Chun LL & Patterson PH (1977). Role of nerve growth factor in the development of rat sympathetic neurons in vitro. III. Effect on acetylcholine production. *J Cell Biol* **75**, 712–718.
- Chung K & Deisseroth K (2013). CLARITY for mapping the nervous system. *Nat Methods* **10**, 508–513.
- Clarke GL, Bhattacharjee A, Tague SE, Hasan W & Smith PG (2010). ss-adrenoceptor blockers increase cardiac sympathetic innervation by inhibiting autoreceptor suppression of axon growth. *J Neurosci* **30**, 12446–12454.
- Costantini I, Ghobril JP, Di Giovanna AP, Allegra Mascaro AL, Silvestri L, Mullenbroich MC, Onofri L, Conti V, Vanzi F, Sacconi L, Guerrini R, Markram H, Iannello G & Pavone FS (2015). A versatile clearing agent for multi-modal brain imaging. *Sci Rep* **5**, 9808.
- Eckberg DL (2000). Physiological basis for human autonomic rhythms. *Ann Med* **32**, 341–349.
- Freeman K, Tao W, Sun H, Soonpaa MH & Rubart M (2014). In situ three-dimensional reconstruction of mouse heart sympathetic innervation by two-photon excitation fluorescence imaging. *J Neurosci Methods* **221**, 48–61.
- Fukuda K, Kanazawa H, Aizawa Y, Ardell JL & Shivkumar K (2015). Cardiac innervation and sudden cardiac death. *Circ Res* **116**, 2005–2019.
- Gramolini AO, Dennis CL, Tinsley JM, Robertson GS, Cartaud J, Davies KE & Jasmin BJ (1997). Local transcriptional control of utrophin expression at the neuromuscular synapse. *J Biol Chem* **272**, 8117–8120.
- Gros D, Jarry-Guichard T, Ten Velde I, de Maziere A, van Kempen MJ, Davoust J, Briand JP, Moorman AF & Jongasma HJ (1994). Restricted distribution of connexin40, a gap junctional protein, in mammalian heart. *Circ Res* **74**, 839–851.
- Grundy D (2015). Principles and standards for reporting animal experiments in The Journal of Physiology and Experimental Physiology. *J Physiol* **593**, 2547–2549.
- Guyton A & Hall J (2006). *Textbook of Medical Physiology*. Elsevier Saunders, Philadelphia, PA.
- Hall ZW & Sanes JR (1993). Synaptic structure and development: the neuromuscular junction. *Cell* **72**(Suppl), 99–121.
- Healy LJ, Jiang Y & Hsu EW (2011). Quantitative comparison of myocardial fiber structure between mice, rabbit, and sheep using diffusion tensor cardiovascular magnetic resonance. *J Cardiovasc Magn Reson* **13**, 74.
- Hoffman JI (1987). Transmural myocardial perfusion. *Prog Cardiovasc Dis* **29**, 429–464.
- Homan AE & Meriney SD (2018). Active zone structure-function relationships at the neuromuscular junction. *Synapse* **72**, e22057.
- Honen BN & Saint DA (2002). Heterogeneity of the properties of INa in epicardial and endocardial cells of rat ventricle. *Clin Exp Pharmacol Physiol* **29**, 161–166.
- Ieda M, Kanazawa H, Kimura K, Hattori F, Ieda Y, Taniguchi M, Lee JK, Matsumura K, Tomita Y, Miyoshi S, Shimoda K, Makino S, Sano M, Kodama I, Ogawa S & Fukuda K (2007). Sema3a maintains normal heart rhythm through sympathetic innervation patterning. *Nat Med* **13**, 604–612.
- Iriki M & Simon E (2012). Differential control of efferent sympathetic activity revisited. *J Physiol Sci* **62**, 275–298.
- Jurevicus J & Fischmeister R (1996). cAMP compartmentation is responsible for a local activation of cardiac Ca²⁺ channels by beta-adrenergic agonists. *PNAS* **93**, 295–299.
- Kimura K, Ieda M & Fukuda K (2012). Development, maturation, and transdifferentiation of cardiac sympathetic nerves. *Circ Res* **110**, 325–336.
- Kreipke RE & Birren SJ (2015). Innervating sympathetic neurons regulate heart size and the timing of cardiomyocyte cell cycle withdrawal. *J Physiol* **593**, 5057–5073.
- Levy MN (1997). Neural control of cardiac function. *Baillieres Clin Neurol* **6**, 227–244.
- Li HH, Kedar V, Zhang C, McDonough H, Arya R, Wang DZ & Patterson C (2004). Atrogin-1/muscle atrophy F-box inhibits calcineurin-dependent cardiac hypertrophy by participating in an SCF ubiquitin ligase complex. *J Clin Invest* **114**, 1058–1071.
- Li L, Desantiago J, Chu G, Kranias EG & Bers DM (2000). Phosphorylation of phospholamban and troponin I in beta-adrenergic-induced acceleration of cardiac relaxation. *Am J Physiol Heart Circ Physiol* **278**, H769–H779.

- Liu DW, Gintant GA & Antzelevitch C (1993). Ionic bases for electrophysiological distinctions among epicardial, midmyocardial, and endocardial myocytes from the free wall of the canine left ventricle. *Circ Res* **72**, 671–687.
- May CN, Frithiof R, Hood SG, McAllen RM, McKinley MJ & Ramchandra R (2010). Specific control of sympathetic nerve activity to the mammalian heart and kidney. *Exp Physiol* **95**, 34–40.
- Mongillo M, McSorley T, Evellin S, Sood A, Lissandron V, Terrin A, Huston E, Hannawacker A, Lohse MJ, Pozzan T, Houslay MD & Zaccolo M (2004). Fluorescence resonance energy transfer-based analysis of cAMP dynamics in live neonatal rat cardiac myocytes reveals distinct functions of compartmentalized phosphodiesterases. *Circ Res* **95**, 67–75.
- Muhlfeld C (2010). High-pressure freezing, chemical fixation and freeze-substitution for immuno-electron microscopy. *Methods Mol Biol* **611**, 87–101.
- Myles RC, Wang L, Kang C, Bers DM & Ripplinger CM (2012). Local beta-adrenergic stimulation overcomes source-sink mismatch to generate focal arrhythmia. *Circ Res* **110**, 1454–1464.
- Nattel S, Rangno RE & Van Loon G (1979). Mechanism of propranolol withdrawal phenomena. *Circulation* **59**, 1158–1164.
- Ogawa S, Barnett JV, Sen L, Galper JB, Smith TW & Marsh JD (1992). Direct contact between sympathetic neurons and rat cardiac myocytes in vitro increases expression of functional calcium channels. *J Clin Invest* **89**, 1085–1093.
- Oh Y, Cho GS, Li Z, Hong I, Zhu R, Kim MJ, Kim YJ, Tampakakis E, Tung L, Huganir R, Dong X, Kwon C & Lee G (2016). Functional coupling with cardiac muscle promotes maturation of hPSC-derived sympathetic neurons. *Cell Stem Cell* **19**, 95–106.
- Perry SJ, Baillie GS, Kohout TA, McPhee I, Magiera MM, Ang KL, Miller WE, McLean AJ, Conti M, Houslay MD & Lefkowitz RJ (2002). Targeting of cyclic AMP degradation to beta 2-adrenergic receptors by beta-arrestins. *Science (New York, NY)* **298**, 834–836.
- Prando V, Da Broi F, Franzoso M, Plazzo AP, Pianca N & Francolini M (2018). Dynamics of neuroeffector coupling at cardiac sympathetic synapses. *J Physiol* **596**, 2055–2075.
- Qu J & Robinson RB (2004). Cardiac ion channel expression and regulation: the role of innervation. *J Mol Cell Cardiol* **37**, 439–448.
- Richards M, Lomas O, Jalink K, Ford KL, Vaughan-Jones RD, Lefkimmatis K & Swietach P (2016). Intracellular tortuosity underlies slow cAMP diffusion in adult ventricular myocytes. *Cardiovasc Res* **110**, 395–407.
- Saggin L, Gorza L, Ausoni S & Schiaffino S (1989). Troponin I switching in the developing heart. *J Biol Chem* **264**, 16299–16302.
- Schaeffer L, de Kerchove d'Exaerde A & Changeux JP (2001). Targeting transcription to the neuromuscular synapse. *Neuron* **31**, 15–22.
- Schneider CA, Rasband WS & Eliceiri KW (2012). NIH Image to ImageJ: 25 years of image analysis. *Nat Methods* **9**, 671–675.
- Shcherbakova OG, Hurt CM, Xiang Y, Dell'Acqua ML, Zhang Q, Tsien RW & Kobilka BK (2007). Organization of beta-adrenoceptor signaling compartments by sympathetic innervation of cardiac myocytes. *J Cell Biol* **176**, 521–533.
- Strom M, Wan X, Poelzing S, Ficker E & Rosenbaum DS (2010). Gap junction heterogeneity as mechanism for electrophysiologically distinct properties across the ventricular wall. *Am J Physiol Heart Circ Physiol* **298**, H787–H794.
- Teutsch C, Kondo RP, Dederko DA, Chrast J, Chien KR & Giles WR (2007). Spatial distributions of Kv4 channels and KChip2 isoforms in the murine heart based on laser capture microdissection. *Cardiovasc Res* **73**, 739–749.
- Thayer JF, Ahs F, Fredrikson M, Sollers JJ, 3rd & Wager TD (2012). A meta-analysis of heart rate variability and neuroimaging studies: implications for heart rate variability as a marker of stress and health. *Neurosci Biobehav Rev* **36**, 747–756.
- Yokoyama T & Lee JK (2017). Quantification of sympathetic hyperinnervation and denervation after myocardial infarction by three-dimensional assessment of the cardiac sympathetic network in cleared transparent murine hearts. *PLoS ONE* **12**, e0182072.
- Zaccolo M & Pozzan T (2002). Discrete microdomains with high concentration of cAMP in stimulated rat neonatal cardiac myocytes. *Science (New York, NY)* **295**, 1711–1715.
- Zaglia T, Di Bona A, Chioato T, Basso C, Ausoni S & Mongillo M (2016). Optimized protocol for immunostaining of experimental GFP-expressing and human hearts. *Histochem Cell Biol* **146**, 407–419.
- Zaglia T, Milan G, Franzoso M, Bertaggia E, Pianca N, Piasentini E, Voltarelli VA, Chiavegato D, Brum PC, Glass DJ, Schiaffino S, Sandri M & Mongillo M (2013). Cardiac sympathetic neurons provide trophic signal to the heart via beta2-adrenoceptor-dependent regulation of proteolysis. *Cardiovasc Res* **97**, 240–250.
- Zaglia T, Milan G, Ruhs A, Franzoso M, Bertaggia E, Pianca N, Carpi A, Carullo P, Pesce P, Sacerdoti D, Sarais C, Catalucci D, Kruger M, Mongillo M & Sandri M (2014). Atrogin-1 deficiency promotes cardiomyopathy and premature death via impaired autophagy. *J Clin Invest* **124**, 2410–2424.
- Zaglia T, Pianca N, Borile G, DaBroi F, Richter C, Campione M, Lehnart SE, Luther S, Corrado D, Miquerol L & Mongillo M (2015). Optogenetic determination of the myocardial requirements for extrasystoles by cell type-specific targeting of ChannelRhodopsin-2. *Proc Natl Acad Sci U S A* **112**, E4495–E4504. <https://doi.org/10.1073/pnas.1509380112>
- Zipes DP (2008). Heart-brain interactions in cardiac arrhythmias: role of the autonomic nervous system. *Cleve Clin J Med* **75**(Suppl 2), S94–S96.

Additional information

Competing interests

The authors declare that they have no competing interests.

Author contributions

NP performed the *in vivo* experiments, as well as the quantitative, biochemical and molecular analyses, and discussed the data. ADB performed analyses on human heart samples, set up the protocol of whole mount staining of neurons and performed multiphoton imaging analysis. EL and IC performed tissue clearing and acquired images. MF performed *in vitro* experiments and contributed to the morphometric analyses. VP performed *in vitro* experiments. AA contributed to the biochemical assays. SR, MF, AA and CB provided autopic human heart samples and contributed to the data discussion. FSP contributed to the whole heart imaging experiments. MR critically discussed the data and performed the 3-D reconstruction of the neuronal network in human samples. LS analysed the CLARITY experiments and contributed to the data discussion and interpretation. TZ and MM designed the study, analysed data and wrote the manuscript. All authors approved the final version of the manuscript submitted for publication and

agree to be accountable for all aspects of the work, in ensuring that questions related to the accuracy or integrity of any part of the work are appropriately investigated and resolved, and that all persons designated as authors qualify for authorship and have been listed.

Funding

This work was supported by the University of Padova (SID2017 to TZ; StarsWiC2017 'miniheartwork' to MM) and ARISLA (pilot grant SNop) to TZ.

Acknowledgements

We are grateful to Dr Marina Campione and Dr Marco Sandri for technical assistance and critical discussion, respectively. Dr David J. Glass provided MuRF1 KO mice. We thank the late Mr Gilberto Benetton for his support.